A Fractional Model of Nonlinear Multi-axial Viscoelastic Behaviors

Anastasia Muliana¹

¹Department of Mechanical Engineering, Texas A&M University, USA

Corresponding author: amuliana@tamu.edu

Abstract

This paper presents a formulation of fractional viscoelasticity of nonlinear time-dependent

responses of isotropic materials undergoing small deformation gradients. The model considers the

separation of functions of the time-dependent kernel and nonlinear elastic strain measure, which

is stress-dependent. The Riemann-Liouville fractional integral is considered for the time-

dependent kernel function. Characterization of material parameters in the fractional viscoelasticity

model is presented using experimental data on a polymer. The non-uniqueness of the calibrated

material parameters from the fractional power terms is discussed. A numerical method is also

presented to solve the nonlinear fractional viscoelastic constitutive model. The response

characteristics and convergence behaviors of the presented nonlinear fractional viscoelastic

constitutive model are compared to the corresponding nonlinear model derived based on classical

viscoelasticity. The presented nonlinear viscoelastic fractional model is shown capable of

describing multi-axial responses of polymers under various loading histories. The fractional model

has significantly fewer material parameters, which can offer an advantage when a relatively long-

term response of materials is of interest. The model is, however, computationally more expensive

when compared to the classical viscoelastic model based on the Prony series kernel function, which

can hinder its practical use in solving rather complex boundary value problems.

1

1. Introduction

Viscoelastic responses of materials when subjected to mechanical stimuli are widely attributed to polymers and biological tissues. Many if not all materials, ranging from biological, geological, and engineered materials to processed food, exhibit viscoelastic responses, even at room temperature. However, in some of these materials, their viscoelastic responses are more pronounced over a relatively long-time span. As such, they are not considered to exhibit viscoelastic responses when investigated under a relatively short time, which is a common time scale for laboratory experiments. The characteristics of viscoelastic materials are typically determined by various parameters, such as viscosity, loss tangent, characteristic of relaxation (or creep) time, relaxation spectrum, etc. For instance, the viscosity of fluid (e.g., air, water, honey, oil, etc.) is typically less than 500 Pa-sec, while the viscosity of polymers can vary from 100 to 106 Pa-sec (Caba and Koch 2015, Hammani et al. 2020). This range of viscosity shows pronounced time-dependent responses of materials in a relatively short time scale (seconds to hours). In contrast to fluid and polymers, the viscosity of the earth mantle is greater than 10¹⁹ Pa-sec (Pollitz et al. 2017), resulting in a slow relaxation behavior for over 10 years. Fused silica glass at room temperature has a viscosity of 10¹⁷-10¹⁸ Pa-sec, indicating a slow relaxation process (Vannoni et al. 2011). This phenomenon can be seen in panes of stained glass in old churches in Europe that are thicker at their bottom due to centuries of a relaxation process from gravitational forces. Structural metals and alloys, such as brass, steel, aluminum alloy, have loss tangent from 10⁻³ to 10⁻⁶ at room temperature, indicating insignificant viscoelastic responses in a short time scale, while the loss tangent of viscoelastic polymers can vary between 0.1 to more than 1 (Lakes and Quackenbush 1996).

The relaxation process in materials is attributed to the motions of the materials' microstructures relative to their neighbors. In polymers, sliding between long chains in amorphous

regions has been the source of polymer relaxation, while in metals the relaxation process is attributed to atom dislocations and/or diffusions. Determining responses of materials under various time scales has been a subject of interest for both fundamental understanding of the process and practical reasons. For this purpose, mathematical models have been formulated to describe viscoelastic responses of materials. Early developments in viscoelasticity considered mechanical analog models with various arrangements of springs and dashpots, e.g., Maxwell, Kelvin-Voigt, Burger, standard linear solid (SLS) models. These models however are limited in capturing responses of materials, particularly when relatively long-term responses are considered. To overcome this issue, multiple spring-dashpot elements have been considered to capture responses from experimental investigations. Several viscoelastic models incorporate the mechanisms of microstructural motions in describing the overall viscoelastic responses of materials [Bergstrom and Boyce 1998, Li et al. 2016]; while other viscoelastic models are phenomenological based, which accounts for the net effect of microstructural motions [Green and Rivlin 1957, Schapery 1969, Pipkin and Rogers 1968, Fung 1981, Rajagopal and Srinivasa 2011, Song et al. 2022, etc.].

In a one-dimensional linear viscoelastic phenomenological model, a minimum of three material parameters are required to describe the overall responses of materials. In this simple linear viscoelastic model, each material parameter has an underlying physical meaning, e.g., instantaneous modulus, relaxed modulus, and characteristic of relaxation time. In many practical situations, larger numbers of material parameters are required to capture the viscoelastic responses of materials, even for a linear viscoelastic response. For this reason, several relaxation (or creep) functions 1, also known as memory kernels, i.e. Prony series, rational polynomial form, fractional power function, etc., have been considered (Blair and Caffyn 1945, William and Watts 1970,

¹ The time-dependent kernel function must be positive, continuous and an increasing function of time in case of creep function while a decreasing function of time for the relaxation function.

Findley et al. 1976). Prony series, which consists of several exponential terms that can be derived from arrangements of multiple spring and dashpot elements, has been widely used due to its flexibility in adding terms to capture time-dependent responses over various time scales, straightforward characterization of material parameters through curve fitting, and fairly easy numerical implementation for computer simulations. The disadvantages of using the Prony series are that a large number of parameters from multiple terms do not have a specific physical attribute that is associated with intrinsic material properties and that there is no uniqueness of the fitted parameters. In practice, it is often convenient to *a priori* set the time parameters for all terms in the Prony series such that each time parameter can capture responses over a certain time window.

To overcome a large number of material parameters in the Prony series, models based on fractional calculus [Bagley and Torvik 1983, Adolfsson et al. 2005] have been considered. Models based on fractional viscoelasticity require few parameters, which can be easily characterized from experimental data that exhibit power-law behaviors [Bonfanti et al. 2020]. As we will discuss later, fractional viscoelastic models have some limitations in incorporating physical meaning into the material parameters. Major drawbacks in fractional viscoelasticity are: it is difficult to numerically implement fractional viscoelastic models and it is computationally expensive [Schmidt and Gaul 2001, Zhang et al. 2020]. Nevertheless, fractional viscoelasticity has been used to describe a wide range of linear viscoelastic materials [Bonfanti et al. 2020].

Linear viscoelasticity² often fails to describe responses of materials over a large range of prescribed external stimuli. Nonlinear viscoelastic models have been formulated to describe time-dependent responses of elastomers, rubbers, polymers, and biological tissues undergoing large

² In a linear viscoelastic material, there are two sources of linearity. A linearized strain measure is used, i.e., only the linear term of the displacement gradients is accounted for. The responses are proportional to the inputs and can be obtained by superimposing the responses of several different inputs. In a linear viscoelastic model, the expression for the time-dependent stress and strain is interchangeable.

deformation gradients [Fung 1981, Bergstrom and Boyce 1998, Muliana et al. 2016], to name a few examples. A viscoelastic material can undergo small-displacement gradients, in which a linearized strain measure is sufficient to describe the deformation of the body; however, its responses may not meet the proportionality and superposition of response. Such material needs to be treated as a nonlinear viscoelastic material, and several constitutive models have been formulated for such nonlinear responses, e.g., [Schapery 1969, Drozdov 1999, Song et al. 2019, Xu et al. 2020]. Like in linear viscoelasticity, when a relatively long-term response is of interest, these nonlinear viscoelastic models often require a large number of parameters to describe the time-dependent responses. The use of fractional calculus in nonlinear viscoelasticity has been limited [Mueller et al. 2011, Mashayekhi et al. 2018, Zhang et al. 2020, Yao et al. 2021].

This study presents a formulation of fractional viscoelasticity of nonlinear time-dependent responses of polymers undergoing small deformation gradients. We present constitutive relations for multi-axial responses of isotropic materials. We discuss the characterization of material parameters in the fractional viscoelasticity model and compare them with the material parameters from a classical nonlinear viscoelastic model. The classical nonlinear viscoelastic model uses the Prony series for the time-dependent kernel. We also present a numerical implementation of the nonlinear fractional viscoelasticity model and assess its computational cost when compared to the classical nonlinear viscoelastic model. While responses of viscoelastic materials can be adequately described by both classical and fractional viscoelastic models, the fractional model is particularly useful when investigating a long-term response of materials as it requires a relatively small number of material parameters. The manuscript is organized as follows. Section two presents constitutive model formulations, followed by material characterizations in Section three. Section four discussed a numerical implementation of the model for describing time-dependent responses of

materials under general loading histories. Finally, Section five is dedicated to discussions and conclusions on the advantage and disadvantages of the use of the fractional viscoelastic model.

2. Constitutive Model Formulation

Pipkin and Rogers (1968) discussed a single integral form of nonlinear viscoelasticity where they described the viscoelastic response of materials with strong nonlinearity using a nonlinear integrand function. This model is based on a modified superposition method, where the stress is expressed in terms of the history of strain. In this study, we adopted the single integral model of Pipkin and Rogers (1968) and considered expressing the strain in terms of the history of stress $\varepsilon(t) = F\left[\sigma(t-s)\right]$, where ε and σ are the linearized strain tensor and Cauchy stress tensor, respectively. The rationale for such a representation is that the stress does not have to be small, but the expression for the function F in terms of the stress leads to a sufficiently small value for the strain. The stress cannot be in general expressed in terms of a nonlinear function of the linearized strain, $\sigma(t) = G\left[\varepsilon(t-s)\right]$, as there is the limitation for the function G that can be chosen; it cannot involve any higher-order terms in ε . A detailed discussion of such a model can be found in Muliana et al. (2013).

The general form of a nonlinear viscoelastic integral model is given as

$$\mathbf{\varepsilon} = \int_{s=0^{-}}^{t} \mathbf{d}_{\mathbf{T}} \mathbf{f}[\mathbf{\sigma}(s), t-s] = \int_{s=0^{-}}^{t} \frac{\partial \mathbf{f}[\mathbf{\sigma}(s), t-s]}{\partial \mathbf{\sigma}(s)} \frac{d\mathbf{\sigma}}{ds} ds$$
 (2.1)

In Eq. (2.1), we consider a separation of functions of the time-dependent kernel and nonlinear elastic strain measure, which is stress-dependent:

$$\mathbf{f}(\mathbf{\sigma}(t),t) = \mathbf{D}(t)\mathbf{F}^{el}(\mathbf{\sigma}) \tag{2.2}$$

Thus, the expression in Eq. (2.1) yields to

$$\mathbf{\varepsilon}(t) = \int_{0^{-}}^{t} \mathbf{D}(t-s) \frac{d\mathbf{F}^{el}(\mathbf{\sigma}(s))}{ds} ds = \int_{0^{-}}^{t} \mathbf{D}(t-s) \frac{\partial \mathbf{F}^{el}(\mathbf{\sigma}(s))}{\partial \mathbf{\sigma}} \frac{d\mathbf{\sigma}}{ds} ds$$
 (2.3)

where $\mathbf{D}(t)$ is the fourth-order tensor of a normalized creep function and $\mathbf{F}^{el}(\sigma)$ is the nonlinear elastic strain measure, expressed in terms of the Cauchy stress tensor. It is noted that the nonlinear elastic strain measure should reduce to zero in absence of stresses $\mathbf{F}^{el}(0) = 0$.

For an isotropic material, the nonlinear elastic strain measure can be written as:

$$\mathbf{F}^{el}(\mathbf{\sigma}(\mathbf{s})) = -f_1(I_1, I_2, I_3)\mathbf{I} + f_2(I_1, I_2, I_3)\mathbf{\sigma}$$
(2.4)

where the functions f_1 and f_2 are expressed in terms of the stress invariants, which are $I_1 = \operatorname{trace}(\sigma), I_2 = \frac{1}{2}\operatorname{trace}(\sigma^2), I_3 = \frac{1}{3}\operatorname{trace}(\sigma^3)$. Here the function f_1 describes the corresponding lateral deformations and portion of the axial deformation due to loading along with the axial directions. The function f_1 does not contribute to any shear deformation. The choice of $f_1(I_1, I_2, I_3)$ and $f_2(I_1, I_2, I_3)$ will be determined from the available experimental data, which will be discussed in Section 3. When upon linearization $\mathbf{F}^{el}(\sigma)$ reduces to a linear elastic response, Eq. (2.3) leads to a linear viscoelastic response. We further consider two normalized time-dependent functions B(t) and J(t) for isotropic materials and Eq. (2.3) becomes:

$$\mathbf{\varepsilon}(t) = -\int_{0^{-}}^{t} B(t-s) \frac{df_{1}(\mathbf{\sigma}(s))}{ds} ds \mathbf{I} + \int_{0^{-}}^{t} J(t-s) \frac{d\left[f_{2}(\mathbf{\sigma}(s))\mathbf{\sigma}(s)\right]}{ds} ds$$
(2.5)

It is noted that by using integral by part, an alternative expression of Eq. (2.5) can be obtained, which can be handy to provide an exact solution or perform numerical integration:

$$\mathbf{\varepsilon}(t) = -B(0)f_1(\mathbf{\sigma}(t))\mathbf{I} - \int_{0^+}^{t} \frac{dB(t-s)}{d(t-s)} f_1(\mathbf{\sigma}(s)) ds \mathbf{I} +$$

$$J(0)f_2(\mathbf{\sigma}(t))\mathbf{\sigma}(t) + \int_{0^+}^{t} \frac{dJ(t-s)}{d(t-s)} f_2(\mathbf{\sigma}(s))\mathbf{\sigma}(s) ds$$
(2.6)

where B(0)=J(0)=1. The expression of the integral model in Eq. (2.5) requires the input history, i.e., the stress history, to be continuous all time within the integral. The integral model in Eq. (2.6) can incorporate a general input history, e.g., in case of a jump discontinuity in describing a creep response.

When only a one-dimensional response is considered, due to normal stress $\sigma(t)$, Eq. (2.4) becomes $f(\sigma) = -f_1(\sigma) + f_2(\sigma)\sigma$ and hence Eq. (2.5) reduces to:

$$\varepsilon(t) = \int_{0^{-}}^{t} D(t-s) \frac{df(\sigma(s))}{ds} ds$$
 (2.7)

where D(t) is a normalized time-dependent creep function, and D(0)=1. Similarly, when only a one-dimensional shear loading $\tau(t)$ is considered, the corresponding shear strain from Eq. (2.5) is

$$\gamma(t) = \int_{0^{-}}^{t} J(t-s) \frac{d\left[f_2(\tau(s))\tau(s)\right]}{ds} ds = \int_{0^{-}}^{t} J(t-s) \frac{dg(\tau(s))}{ds} ds$$
 (2.8)

The next step is to define the forms for the time-dependent kernel functions. To motivate the discussion, we will start with a one-dimensional response, followed by a multi-axial response.

2.1 One-dimensional response

To define the fractional viscoelastic model utilizing the creep function, we adopt the Riemann-Liouville fractional integral, which is defined as follow:

$${}_{c}I_{t}^{\alpha}f(t) = \frac{1}{\Gamma(\alpha)} \int_{c}^{t} (t-s)^{\alpha-1} f(s)ds, \quad t > c, \quad \alpha \in \mathbb{R}, \quad \alpha > 0$$
 (2.9)

where $\Gamma(\bullet)$ is the Gamma function. The fractional operators are nonlocal in nature, in which they account for hereditary information in determining the response characteristics of certain phenomena. Thus, they are suitable to describe responses of materials with history dependences. We take c=0 and consider $\beta=\alpha-1$, Eq. (2.9) becomes:

$${}_{0}I_{t}^{\beta}f(t) = \frac{1}{\Gamma(\beta+1)} \int_{0}^{t} (t-s)^{\beta} f(s)ds, \quad t > 0, \quad \beta \in \mathbb{R}, \quad \beta > 0$$
 (2.10)

The expression in Eq. (2.10) can be used to represent time-dependent strain with a power-law creep function. Experimental observation on creep responses showed that the creep compliance can be expressed by a power function of time i.e., $\Delta D(t) = Ct^{\beta}$, $\beta > 0$, where C and β are material parameters, see for example Harper and Weitsman (1985). By adopting the fractional integral in Eq. (2.10), the normalized time-dependent creep function in Eq. (2.7) can now be written as:

$$D(t) = D(0) + \frac{D_{\beta}}{\Gamma(\beta + 1)} t^{\beta}$$
(2.11)

The creep function in Eq. (2.11) includes a jump discontinuity at time 0, which is attributed to the instantaneous elastic response. Two material parameters D_{β} and β need to be calibrated from experimental tests. It can be seen in Eq. (2.11) that β =0 gives the response of an elastic solid while β =1 results in the response of a viscous fluid. As has been discussed in the literature [Bonfanti et al. 2020], it is often necessary to consider more than one power term to capture the entire creep responses, and thus Eq. (2.11) can be expanded as:

$$D(t) = D(0) + \sum_{n=1}^{N} \frac{D_{\beta_n}}{\Gamma(\beta_n + 1)} t^{\beta_n}$$
(2.12)

By substituting Eq. (2.12) into Eq. (2.7), the one-dimensional strain of a nonlinear fractional viscoelasticity model is given as:

$$\varepsilon(t) = D(0)f(\sigma(t)) + \int_{0}^{t} \sum_{n=1}^{N} \frac{D_{\beta_n}(t-s)^{\beta_n}}{\Gamma(\beta_n+1)} \frac{df(\sigma(s))}{ds} ds$$
 (2.13)

When multiple terms are considered, the lower value of the power β_n describes responses at an early time (short-term response), while the higher value of β_n captures responses at a later time (long-term response). This behavior is similar to the use of the Prony series for the kernel function, as each parameter in the exponent represents the dominant response at a certain time domain.

2.2 Multi-axial response

The multi-axial responses for the isotropic fractional viscoelastic model are formed by defining the normalized time-dependent creep functions B(t) and J(t) as follows:

$$B(t) = B(0) + \sum_{n=1}^{N} \frac{B_{\delta_n}}{\Gamma(\delta_n + 1)} t^{\delta_n}$$
(2.14)

$$J(t) = J(0) + \sum_{m=1}^{M} \frac{J_{\lambda_m}}{\Gamma(\lambda_m + 1)} t^{\lambda_m}$$
 (2.15)

where N and M are numbers of terms in the time-dependent bulk and shear functions, respectively, and B_{δ_n} , δ_n , J_{λ_m} , λ_m are material parameters to be calibrated from experimental data. Using the creep functions in Eqs. (2.14) and (2.15), the time-dependent strain in Eq. (2.5) are rewritten as:

$$\mathbf{\varepsilon}(t) = -B(0)f_1(\mathbf{\sigma}(t)\mathbf{I} - \int_0^t \sum_{n=1}^N \frac{B_{\delta_n}}{\Gamma(\delta_n + 1)} (t - s)^{\delta_n} \frac{df_1(\mathbf{\sigma}(s))}{ds} ds \mathbf{I} +$$

$$J(0)f_2(\mathbf{\sigma}(t))\mathbf{\sigma}(t) + \int_0^t \sum_{m=1}^M \frac{J_{\lambda_m}}{\Gamma(\lambda_m + 1)} (t - s)^{\lambda_m} \frac{d[f_2(\mathbf{\sigma}(s))\mathbf{\sigma}(s)]}{ds} ds$$
(2.16)

When the expression of the time-dependent strain in Eq. (2.6) is used instead, we have

$$\mathbf{\varepsilon}(t) = -B(0)f_{1}(\mathbf{\sigma}(t))\mathbf{I} - \int_{0^{+}}^{t} \sum_{n=1}^{N} \frac{B_{\delta_{n}}}{\Gamma(\delta_{n}+1)} \delta_{n}(t-s)^{\delta_{n}-1} f_{1}(\mathbf{\sigma}(s)) ds \mathbf{I} +$$

$$J(0)f_{2}(\mathbf{\sigma}(t))\mathbf{\sigma}(t) + \int_{0^{+}}^{t} \sum_{m=1}^{M} \frac{J_{\lambda_{m}}}{\Gamma(\lambda_{m}+1)} \lambda_{m}(t-s)^{\lambda_{m}-1} f_{2}(\mathbf{\sigma}(s))\mathbf{\sigma}(s) ds$$

$$(2.17)$$

When the second term of Eq. (2.14) and Eq. (2.15) is absent or when we evaluate at time t=0, the strain expression in both Eqs. (2.16) and (2.17), noted that B(0)=J(0)=1, reduces to a nonlinear elastic response,

$$\mathbf{\varepsilon}(t) = -f_1(\mathbf{\sigma}(t))\mathbf{I} + f_2(\mathbf{\sigma}(t))\mathbf{\sigma}(t) \tag{2.18}$$

Linear elastic response for isotropic materials is described by $f_1(\mathbf{\sigma}) = -\frac{v}{E} trace(\mathbf{\sigma}); \ f_2(\mathbf{\sigma}) = \frac{1+v}{E},$ where E and v are the elastic modulus and Poisson's ratio, respectively.

3. Material Parameter Characterization and Model Predictions

We now present a discussion on material parameter characterizations in the fractional viscoelastic model, both for one-dimensional and multi-axial cases, and compare them with the ones determined from the Prony series of classical viscoelasticity. The one-dimensional response is used to facilitate the discussion and comparison with the classical viscoelasticity. Responses of polyoxymethylene (POM) polymer are used. The experimental test is presented in the **Appendix**.

3.1 One dimensional material characterization

rate $\dot{\sigma}$ and the other is a creep test under a constant stress σ_0 . If it is assumed that the ramp loading is conducted at a relatively fast rate so that the time-dependent effect is insignificant, then from the ramp loading response, i.e., a stress-strain relation, we can determine the nonlinear function $f(\sigma)$, which is an elastic strain. To illustrate this idea, consider a material with a characteristic of creep time τ_0 , and the ramp loading takes place until time t^* . At time t^* , let say we have stress σ_0 and its rate $\dot{\sigma}_0$, thus $\frac{\dot{\sigma}_0}{\sigma_0} = \frac{1}{t^*}$. If the time t^* is small compared to the characteristics of creep time, $\frac{\dot{\sigma}_0}{\sigma_0} \tau_c \gg 1$ and $\frac{t^*}{\tau_c} \ll 1$, thus $\varepsilon(t^*) \approx f(\sigma(t^*))^3$. In such a situation, the nonlinear plot of a stress-strain, Fig. 1 top, is not attributed to the stress relaxation (or creep) process. In Fig. 1 top, POM specimens were subjected to a uniaxial ramp test with constant stress rates of 2.5 MPa/sec and 25 MPa/sec, which show an insignificant effect of loading rates in these ranges of stress rates. The response under a quasi-static ramp was used to determine $f(\sigma(t))$.

Consider a simple uniaxial test under two loading histories. One is a ramp loading with a stress

POM experiences creep when the stress is held for a period of time, see Fig. 1 bottom. During a creep experiment, the specimen is ramped to a stress state before the stress is held constant. The time-dependent material parameters are typically characterized from the creep portion of the data, which implies that the ramp portion has an insignificant time-dependent

 $^{^{3}}$ Let us define the normalized time history $\hat{s}=s$ / au_{c} , and the second term of Eq. (2.13) becomes

 $[\]int_{0}^{t^*/\tau_c} D\left(\frac{t}{\tau_c} - \hat{s}\right) \frac{df}{d\sigma} \frac{d\sigma}{d\hat{s}} \tau_c d\hat{s} \approx 0.$

response. For this to be true, it is then necessary to apply the load sufficiently fast during the ramp. Otherwise, the time-dependent parameters need to be calibrated from the entire loading history. Considering a jump discontinuity in the stress at an initial time t=0, the corresponding creep strain from Eq. (2.2) is $\varepsilon(\sigma_o, t) = D(t) f(\sigma_o)$.

For the studied POM polymer, the following function is used to capture the nonlinear elastic response of the material in Fig. 1 top.

$$f(\sigma) = A \left(e^{B\sqrt{\sigma^2}} - 1 \right) \tag{3.1}$$

where A and B are the material parameters that need to be determined from the experiment. For the studied POM, the calibrated values are $A = 7.5 \times 10^{-3}$; B = 0.03. It is noted that upon linearization, Eq. (2.20) reduces to $\varepsilon = \frac{df}{d\sigma}\Big|_{\sigma=0} \sigma = AB\sigma = \frac{1}{E}\sigma$, where E=4444 MPa is the elastic modulus of the material.

Next, we calibrate material parameters in the time-dependent creep function. For this purpose, a normalized creep compliance response is obtained from the creep strain data. The creep test was conducted by ramping the stress with a constant rate of 5 MPa/sec to stress ~30 MPa, and thus the rise time $t^*=\sim 6$ sec. The normalized creep compliance is obtained from $D(t)=\frac{\mathcal{E}(t)}{\mathcal{E}(t^*)}$, as shown in **Fig. 2**. We consider both one power term and two power terms for the normalized time-dependent function with the calibrated parameters listed in **Table 1**. It is seen that two power terms are needed to better capture the entire creep responses, both at early and later creep responses. We also compare the calibration using the Prony series (shown in **Table 2**), which is referred to as the classical viscoelastic model. The fractional viscoelastic model requires fewer numbers of parameters to be calibrated from experiments when compared to the classical viscoelastic model.

In both models, there is no uniqueness in the time-dependent material parameters. **Table 3** presents several sets of material parameters in the fractional viscoelastic model that can capture the experimental data including the calculated root mean square errors when compared to the creep responses from Trial 1. **Figure 3** shows the time-dependent kernel responses from three sets of material parameters. Likewise, for the classical viscoelastic model different sets of Prony parameters can be used to describe the time-dependent compliance.

One of the limitations of the fractional viscoelastic kernel is that the material parameters lack physical meaning. The memory kernel for the creep compliance in Eq. (2.12) has material parameters D_{β_n} whose unit would change with the power value of β_n , e.g., sec- β_n , and thus no physical meaning can be attributed to these material parameters. This issue has been discussed in Bonvanti et al. (2020). In the classical viscoelastic model using a series of exponential functions, the different exponential terms represent the relative dominant creep/relaxation behavior at different times. The two parameters in each exponential term are measures of modulus (or compliance) and time, although they do not represent any intrinsic material properties.

The creep-recovery strain responses in **Fig. 1 bottom** is now described by:

$$\varepsilon(t) = \begin{cases} f(\sigma_o)D(t), & 0 \le t < t_R \\ f(\sigma_o)[D(t) - D(t - t_R)], & t \ge t_R \end{cases}$$

$$D(t) = 1 + \frac{D_{\beta_1}}{\Gamma(1 + \beta_1)} t^{\beta_1} + \frac{D_{\beta_2}}{\Gamma(1 + \beta_2)} t^{\beta_2}$$
(3.2)

where the recovery time t_R is the time at which the load is removed. During the experiment, the load removal was performed at a rate of 10 MPa/sec. The simulation was performed by considering a step loading and unloading, instead of carrying out an actual loading history (ramp loading – hold – ramp unloading – hold).

3.2 Multi-axial material characterization

To determine the multi-axial material parameters for the isotropic viscoelastic material, uniaxial tensile test data under two loading histories, which are a quasi-static ramp at a relatively fast rate and creep at constant stress were used. The axial and lateral displacements were recorded and the corresponding axial and lateral strains were obtained. Similar to the one-dimensional case, the responses from the ramp loading were used to determine the nonlinear elastic response while the creep data were used to calibrate the time-dependent parameters.

Figure 4 illustrates the axial and lateral responses from a quasi-static ramp loading at a fast rate of 25 MPa/sec. The following functions⁴ are considered for the nonlinear elastic strain measure in Eq. (2.4):

$$f_1(\mathbf{\sigma}) = A \left[\exp\left(B\sqrt{(I_1)^2}\right) - 1 \right] \frac{I_1}{|I_1|}$$
(3.3)

$$f_2(\mathbf{\sigma}) = C \left[\frac{\exp\left(D\sqrt{2I_2}\right) - 1}{\sqrt{2I_2}} \right]$$
 (3.4)

Four material parameters need to be calibrated from the experiments. The two parameters A and B in Eq. (3.3) were first determined from the lateral stress-strain plot in **Fig. 4**, followed by the determination of C and D in Eq. (3.4) from the axial stress-strain plot. Under a uniaxial tensile loading, the only nonzero stress is $\sigma_{11}(t) = \sigma(t)$, and hence $I_1 = \sigma(t)$ and $I_2 = 0.5(\sigma(t))^2$. The axial and lateral elastic strains are given as:

$$\varepsilon_{22}(\sigma) = \varepsilon_{33}(\sigma) = -A \left[\exp(B\sigma) - 1 \right]$$
 (3.5)

15

⁴ In the limit of the denominator going to zero $\lim_{x\to 0}\frac{e^{\lambda x}-1}{x}=\lim_{x\to 0}\frac{\lambda e^{\lambda x}}{1}=\lambda$. Since λ is constant, and at zero stresses, λ 0=0.

$$\varepsilon_{11}(\sigma) = -A \left[\exp(B\sigma) - 1 \right] + C \left[\exp(D\sigma) - 1 \right]$$
 (3.6)

The calibrated material parameters are $A=1.8 \times 10^{-3}$; B=0.0365; $C=7.8 \times 10^{-3}$; D=0.0345. Upon linearization, linear elastic material properties can be obtained as $AB=\frac{v}{E}$; $CD=\frac{1+v}{E}$, which give E=4916 MPa and v=0.32.

The time-dependent parameters are determined from the normalized creep data. As discussed in the one-dimensional parameter characterization, the lateral and axial creep strains are determined by considering a step loading, which are given as:

$$\varepsilon_{22}(t) = \varepsilon_{33}(t) = -f_1(\sigma_o)B(t) \tag{3.7}$$

$$\varepsilon_{11}(t) = -f_1(\sigma_0)B(t) + f_2(\sigma_0)\sigma_0 J(t) \tag{3.8}$$

where

$$B(t) = 1 + \frac{B_{\delta_1}}{\Gamma(1+\delta_1)} t^{\delta_1} + \frac{B_{\delta_2}}{\Gamma(1+\delta_2)} t^{\delta_2}$$
(3.9)

$$J(t) = 1 + \frac{J_{\lambda_1}}{\Gamma(1+\lambda_1)} t^{\lambda_1} + \frac{J_{\lambda_2}}{\Gamma(1+\lambda_2)} t^{\lambda_2}$$
(3.10)

From the lateral creep response (**Fig. 5 bottom**), the time-dependent function B(t) can be characterized, followed by the characterization of J(t) from the axial creep response (**Fig. 5 top**). The calibrated parameters are given in **Table 4**. Next, the recovery responses are predicted from the following models:

$$\varepsilon_{22}(t) = \varepsilon_{33}(t) = -f_1(\sigma_0) (B(t) - B(t - t_R)), \quad t \ge t_R$$
(3.11)

$$\varepsilon_{11}(t) = -f_1(\sigma_0) \left(B(t) - B(t - t_R) \right) + f_2(\sigma_0) \sigma_0 \left(J(t) - J(t - t_R) \right), \quad t \ge t_R \quad (3.12)$$

Figure 5 shows the axial and lateral creep-recovery responses under the constant stress of 20 MPa. During the material calibration process, a step loading and unloading history was considered. The

root mean square (RMS) difference between the model prediction and experiment for the axial and transverse strain responses are 0.0122% and 0.0158%, respectively.

4. Numerical Implementation and Structural Analyses

The above analytical models on predicting the creep and recovery strain responses are easily obtained under a relatively simple loading history. Under a more general loading history and/or more complex boundary conditions, a general expression of the viscoelastic fractional model, either from Eq. (2.16) or Eq. (2.17) is required. Depending on the complexities of the nonlinear elastic functions, loading histories, and boundary conditions, it is not always possible to find exact solutions to these integral models. In such situations, numerical methods are often sought.

The bottleneck of using fractional viscoelasticity is in performing numerical analyses. In the classical viscoelasticity that uses the Prony series, a recursive method has been employed to solve the integral equations that enable carrying the histories from the previous time step [Taylor et al. 1970, Henriksen 1984, Haj-Ali and Muliana 2004, Petterman and DeSimone 2018]. This method reduces storage of history variables and computational costs, although it is argued that a large number of terms in the Prony series can increase computational costs especially for running large-scale simulations. In fractional viscoelasticity models, numerical integrations are often done by cumulative approximations that require calculating responses from the initial loading stage [Schmidt and Gaul 2001, Garra et al. 2017]. This, in fact, tremendously increases the computational cost even when the fractional viscoelasticity model has much fewer material parameters compared to the classical viscoelasticity that uses the Prony series. To overcome the complexities in performing numerical analyses for fractional viscoelasticity, Zhang et al. (2020) have adopted a recursive approximation, in which they used the Prony series to approximate the

fractional derivatives. By doing so, there is a need to determine the parameters in the Prony series, which might defeat the initial purpose to replace the classical viscoelasticity with fractional viscoelasticity, although the proposed numerical scheme is computationally efficient and suitable for large scale simulation. The use of a recursive approach in solving the Caputo derivative was also used by Yuan and Agrawal (2002), where they used Gauss-Laguerre quadrature for performing numerical integration. However, this approach suffers from slow convergence when the integrand is non-smooth.

In this study, we consider using a cumulative approximation to integrate the fractional viscoelasticity model. We once again started with the one-dimensional case to highlight the computational procedure and assess the computational cost as compared to the recursive method used for the classical viscoelasticity. We then perform the numerical integration for the multi-axial model and use them to simulate various loading histories.

We consider the fractional viscoelasticity model expressed in Eq. (2.17), where for a onedimensional case reduces to:

$$\varepsilon(t) = D(0)f(\sigma(t)) + \int_{0}^{t} \sum_{n=1}^{N} \frac{D_{\beta_n} \beta_n (t-s)^{\beta_n - 1}}{\Gamma(\beta_n + 1)} f(\sigma(s)) ds$$

$$\tag{4.1}$$

with $f(\sigma)$ is given in Eq. (3.1). The second term of Eq. (4.1) is approximated as

$$\int_{0}^{t} \sum_{n=1}^{N} \frac{D_{\beta_n} \beta_n (t-s)^{\beta_n - 1}}{\Gamma(\beta_n + 1)} f(\sigma(s)) ds \approx \sum_{n=1}^{N} \frac{D_{\beta_n} \beta_n}{\Gamma(\beta_n + 1)} \sum_{k=0}^{K} (t - t_k)^{\beta_n - 1} f\left(\sigma\left(t_k + \frac{\Delta t}{2}\right)\right) \Delta t \tag{4.2}$$

where $K = t / \Delta t$ and mid-point integration is used.

Compared to the classical viscoelasticity using Prony series term for the time-dependent function, a recursive method is used to integrate the constitutive relation, which is summarized as:

$$\varepsilon(t) = D(0)f(\sigma(t)) + \int_{0}^{t} \sum_{n=1}^{N_p} \frac{D_n}{\tau_n} e^{-(t-s)/\tau_n} f(\sigma(s)) ds = D(0)f(\sigma(t)) + \sum_{n=1}^{N_p} q_n(t)$$
(4.3)

$$q_n(t) \approx e^{-\Delta t/\tau_n} q_n(t - \Delta t) + \frac{D_n}{\tau_n} \frac{\Delta t}{2} \left(f(\sigma(t)) + e^{-\Delta t/\tau_n} f(\sigma(t - \Delta t)) \right)$$
(4.4)

where $q_n(t)$ is the history variable for each Prony term that needs to be stored to be used for the next time step. It is seen that even when storage is needed to store the history variable for each term in the Prony series, it is not necessary to compute cumulative responses from the beginning of loading at each time step, unlike the method used in Eq. (4.2). The use of the exponential function for the time kernel enables to use recursive integration method.

Both integration methods for the classical and fractional viscoelasticity models are implemented in MATLAB software (R2016b). In both models, a mid-point method is used to approximate the integration within each time increment. We now compare the accuracy and computational cost of the two methods. We first consider a creep loading history with a ramp at constant stress until a rise time $t^*=1$ sec and the stress is 20 MPa, the stress is held constant for the next 600 minutes (36000 seconds). A convergence study was first performed in determining the time increment that gives a good approximation of the responses. **Figure 6** shows the responses from the fractional viscoelasticity and classical viscoelasticity models with several time increments. The computational costs in all cases are given in **Table 5**. The RMS of the differences in strain responses from the numerical and analytical solutions is also shown in **Fig. 6**. The convergence in using the cumulative approach in integrating the function is quite slow and also required significantly high computational costs compared to the use of the recursive approach. The slow convergence and high computational cost in the fractional viscoelastic model can hinder its practical use when solving a rather complex boundary value problems is needed.

We also compare the numerical responses from the classical and fractional viscoelastic models under cyclic loading, $\sigma(t) = 50 \sin\left(\frac{2\pi}{T}t\right)$ MPa, where T is the period of loading. **Figure** 7 shows the cyclic responses from the two models at different periods. A time increment of 1 second was used for both classical and fractional viscoelasticity models. The RMS of strain responses obtained from the fractional and classical viscoelastic models for loading under periods 60 sec and 3600 sec are 0.0247% and 0.0235%, respectively.

For the multi-axial case, the model in Eq. (2.17) is now approximated as:

$$\mathbf{\varepsilon}(t) \approx -B(0)f_{1}(\mathbf{\sigma}(t))\mathbf{I} - \sum_{n=1}^{N} \frac{B_{\delta_{n}} \delta_{n}}{\Gamma(\delta_{n}+1)} \sum_{k=0}^{K} (t - t_{k})^{\delta_{n}-1} f_{1}\left(\mathbf{\sigma}\left(t_{k} + \frac{\Delta t}{2}\right)\right) \Delta t \mathbf{I}$$

$$J(0)f_{2}(\mathbf{\sigma}(t))\mathbf{\sigma}(t) + \sum_{n=1}^{N} \frac{J_{\lambda_{n}} \lambda_{n}}{\Gamma(\lambda_{n}+1)} \sum_{k=0}^{K} (t - t_{k})^{\lambda_{n}-1} f_{2}\left(\mathbf{\sigma}\left(t_{k} + \frac{\Delta t}{2}\right)\right) \mathbf{\sigma}\left(t_{k} + \frac{\Delta t}{2}\right) \Delta t$$

$$(4.5)$$

Figure 8 shows the numerical predictions of the creep-recovery responses obtained from the fractional viscoelastic model. The rate during the loading and unloading ramps was at 5 MPa/sec and a time increment of 1 second was used in the simulation. The RMS between the model prediction and experiment for the axial and transverse strain responses are 0.0175% and 0.0222%, respectively.

Finally, we present an analysis of a pressurized cylinder subjected to an inner pressure $p_i(t)$. The cylinder has inner and outer radii of 80 mm and 100 mm, respectively. The corresponding radial and circumferential stresses are:

$$\sigma_{rr}(r,t) = \frac{p_i(t)r_i^2}{r_o^2 - r_i^2} \left(1 - \frac{r_o^2}{r^2} \right); \qquad \sigma_{\theta\theta}(r,t) = \frac{p_i(t)r_i^2}{r_o^2 - r_i^2} \left(1 + \frac{r_o^2}{r^2} \right)$$
(4.6)

The corresponding radial and circumferential strains are:

$$\varepsilon_{rr}(r,t) = -B(0)f_{1}(\mathbf{\sigma}(t))\mathbf{I} - \int_{0^{+}}^{t} \sum_{n=1}^{N} \frac{B_{\delta_{n}}}{\Gamma(\delta_{n}+1)} \delta_{n}(t-s)^{\delta_{n}-1} f_{1}(\mathbf{\sigma}(s)) ds \mathbf{I} +$$

$$J(0)f_{2}(\mathbf{\sigma}(t))\sigma_{rr}(r,t) + \int_{0^{+}}^{t} \sum_{m=1}^{M} \frac{J_{\lambda_{m}}}{\Gamma(\lambda_{m}+1)} \lambda_{m}(t-s)^{\lambda_{m}-1} f_{2}(\mathbf{\sigma}(s))\sigma_{rr}(r,s) ds$$

$$(4.7)$$

$$\varepsilon_{\theta\theta}(r,t) = -B(0)f_{1}(\mathbf{\sigma}(t))\mathbf{I} - \int_{0^{+}}^{t} \sum_{n=1}^{N} \frac{B_{\delta_{n}}}{\Gamma(\delta_{n}+1)} \delta_{n}(t-s)^{\delta_{n}-1} f_{1}(\mathbf{\sigma}(s)) ds \mathbf{I} +$$

$$J(0)f_{2}(\mathbf{\sigma}(t))\sigma_{\theta\theta}(r,t) + \int_{0^{+}}^{t} \sum_{m=1}^{M} \frac{J_{\lambda_{m}}}{\Gamma(\lambda_{m}+1)} \lambda_{m}(t-s)^{\lambda_{m}-1} f_{2}(\mathbf{\sigma}(s))\sigma_{\theta\theta}(r,s) ds$$

$$(4.9)$$

where the nonlinear functions are given in Eqs. (3.3) and (3.4) with the following invariants:

$$I_1(r,t) = \sigma_{rr}(r,t) + \sigma_{\theta\theta}(r,t); \quad I_2(r,t) = 2\left(\sigma_{rr}^2(r,t) + \sigma_{\theta\theta}^2(r,t)\right)$$
 (4.10)

We compute the corresponding radial displacement as:

$$u_r(r,t) = r\varepsilon_{\theta\theta}(r,t) = \int_0^r \varepsilon_{rr}(\varsigma,t)d\varsigma$$
(4.11)

Figure 9 illustrates the time-dependent radial displacement at the inner surface of the cylinder under two different pressures 5 and 10 MPa, highlighting the nonlinear viscoelastic response of the material when compared to a linear viscoelastic response. The radial and circumferential distributions for the two pressures are shown in **Fig. 10**, indicating relatively large stresses beyond a linear viscoelastic response of the material. The temporal and spatial variations of the radial displacements at the two pressures are depicted in **Fig. 11**.

5. Discussions and Conclusions

We have presented a fractional integral model for describing the multi-axial nonlinear viscoelastic response of materials undergoing small deformation gradients. The model is suitable for isotropic

material behaviors. The model considers the separation of functions of the time-dependent kernel and nonlinear elastic strain measure. The fractional integral function is used for the normalized time-dependent kernel. The nonlinear elastic strain measure is stress-dependent and different functions can be considered for the nonlinear elastic strain measure with a requirement that the nonlinear elastic strain measure should reduce to zero in absence of stresses. The function for the nonlinear strain measure can be determined from available experimental data. We use experimental data on a POM polymer to show the calibration of the material parameters in the model and validate the model. The experimental data under quasi-static ramp loadings at relatively fast loading rate, where the time-dependent effect is insignificant, are used to determine the nonlinear elastic strain measure while the relatively long-term creep data (24 hours or 1440 minutes) are used to determine the parameters in the time-dependent kernel function. Responses from both axial and lateral deformations are used to characterize the multi-axial response of the materials. In this study, two terms of fractional power are considered and the material parameters in these two terms are not unique as multiple parameter combinations can adequately capture the entire time-dependent response of the materials. In all studies presented here, the RMS differences of strains obtained from the fractional model and experimental data and also when comparing the strain predictions from the fractional and classical models are less than 0.025%. The fractional viscoelastic model requires significantly a smaller number of material parameters (4 parameters) when compared to the classical viscoelastic model using the Prony parameters (10 parameters), which is one of the advantages of the fractional viscoelastic model. Although the parameters in the fractional model are not unique, a smaller number of parameters is particularly useful when trying to understand time-dependent responses of new materials, examining the implication of short

and/or long-term material responses on certain performance characteristics, and designing materials with desired time-dependent response characteristics.

We also present a numerical integration method to solve the fractional integral model. A cumulative approximation that requires calculating responses from the initial loading stage and a mid-point integration are considered to integrate the fractional viscoelasticity model, which tremendously increases the computational cost even when the fractional viscoelasticity model has much fewer material parameters compared to the classical viscoelasticity that uses the Prony series. The cumulative approximation also shows slow convergence behaviors when compared to the recursive integration method in the classical viscoelasticity model. The slow convergence and high computational cost in the fractional viscoelastic model can hinder its practical use when solving a rather complex boundary value problems is needed.

Acknowledgment

The research work of this paper was performed within the framework of the COMET-program of the Austrian Ministry of Traffic, Innovation, and Technology. We would like to thank Dr. Daniel Tscharnuter for carrying out the experimental test. This work was partly supported by the National Science Foundation under grant CMMI-1761015.

Reference

- 1. Adolfsson K, Enelund M, and Olsson P (2005), "On the Fractional Order Model of Viscoelasticity" Mechanics of Time-dependent Materials, 9, pp. 15-35
- 2. Bagley RL and Torvik PJ (1983), "Fractional Calculus A Different Approach to the Analysis of Viscoelastically Damped Structures" AIAA Journal, 21, pp. 741-748
- 3. Bergstrom JS and Boyce MC (1998), "Constitutive Modeling of the Large Strain Time-dependent Behavior of Elastomers," J. Mechanics Physics of Solids, 46, pp. 931-954
- 4. Blair GS and Caffyn J (1945), Significance of power-law relations in rheology, Nature, vol. 155, pp. 171–172

- 5. Bonfanti A, Kaplan JL, Charras G, and Kabla A (2020), "Fractional Viscoelastic Modes for Power-law Materials" Soft Matter, 16, pp. 6002-6020
- 6. Caba S and Koch M (2015), "Modeling the Viscosity Development of Epoxy Resins during Injection of the RTM Process" Proceedings of the Regional Conference, Polymer Processing Society, PPS, AIP Conf. Proceeding 1779, 070002
- 7. Drozdov, A. (1999), "A Constitutive Model in Viscoelastoplasticity of Glassy Polymers," Polymer, 40, pp. 3711-3727
- 8. Findley, W.N., Lai, J.S., and Onaran, K (1976), "Creep and Relaxation of Nonlinear Viscoelastic Materials," New York, Dover Publication
- 9. Fung YC, Biomechanics: Mechanical Properties of Living Tissues, Springer, New York 1981
- 10. Garra R, Mainardi F, Spada G (2017), "A generalization of the Lomnitz logarithmic creep law via Hadamard fractional calculus" Chaos, Solitons, and Fractals, 102, pp. 333-338
- 11. Green AE and Rivlin RS (1957), "The mechanics of non-linear materials with memory," Archive for Rational Mechanics and Analysis 1 (1) (1957) 1–21
- 12. Hammani S, Moulai-Mostefa N, Samyn P, Becgelany M, Dufresne A, and Barhoum A (2020), "Morphology, Rheology and Crystallization in Relation to the Viscosity Ratio of Polystyrene/Polypropylene Polymer Blends" Materials, 13, 926, 20 pages
- 13. Harper, B. D. and Weitsman, Y. (1985), "Characterization Method for a Class of Thermorheologically Complex Materials," J. of Rheology, 29, pp. 49-66
- 14. Lakes RS and Quackenbush J (1996), "Viscoelastic Behaviour in Indium Tin Alloys over a Wide Range of Frequency and Time" Philosophical Magazine Letters, 74, 227-232
- 15. Li Y, Tang S, Kroger M, and Liu WK (2016), "Molecular Simulation Guided Constitutive Modeling on Finite Strain Viscoelasticity of Elastomers" J. Mechanics and Physics of Solids, 88, pp. 204-226
- 16. Mashayekhi S, Miles P, Hussaini MY, Oates W (2018), "Fractional Viscoelasticity in Fractal and Non-Fractal Media: Theory, Experiment, Validation, and Uncertainty Analysis" J. Mechanics and Physics of Solids, 111, pp. 134-156
- Mueler S, Kaestner M, Brummund J, Ulbricht V (2011), "A Nonlinear Fractional Viscoelastic Material Model for Polymers" Computational Material Science, 50, pp. 2938-2949
- 18. Muliana A, Rajagopal KR, Wineman AS (2013), "A New Class of Quasi-Linear Models for Describing the Nonlinear Viscoelastic Response of Materials" Acta Mechanica, 224, pp. 2169-2183
- 19. Muliana A, Rajagopal KR, Tscharnuter D, Pinter G (2016), "A Nonlinear Viscoelastic Constitutive Model of Polymeric Solids based on Multiple Natural Configuration Theory" International Journal of Solids and Structures, 100, pp. 95-110
- Petterman H and DeSimone A (2018), "An Anisotropic Linear Thermo-viscoelastic Constitutive Law: Elastic Relaxation and Thermal Expansion Creep in the Time Domain" Mech. Time-dependent Materials, 22, 421-433
- 21. Pipkin AC and Rogers TG (1968), "A Non-linear Integral Representation for Viscoelastic Behaviour" Journal of the Mechanics and Physics of Solids, 16, pp. 59–72
- 22. Pollitz FF, Kobahashi T, Yarai H, Shibazaki B, and Matsumoto T (2017), "Viscoelastic Lower Crust and Mantle Relaxation Following the 14-16 April 2016 Kumamoto, Japan Earthquake Sequence" Geophysical Research Letters, 44, 8795-8803

- 23. Rajagopal KR and Srinivasa AS (2011), "A gibbs-potential-based formulation for obtaining the response functions for a class of viscoelastic materials," Proceedings of the Royal Society of London A: Mathematical, Physical and Engineering Sciences 467 (2125), 39–58
- 24. Schapery RA (1969) "On the Characterization of Nonlinear Viscoelastic Materials," Polymer Engineering and Science, Vol. 9, No. 4, pp. 295-310
- 25. Schmidt A and Gaul L (2001), "FE Implementation of Viscoelastic Constitutive Stress-strain Relations Involving Fractional Time Derivatives" Constitutive Models for Rubber II, AA Balkema Publishers, Tokyo, S. 79-89
- 26. Song R, Rajagopal, KR, and Muliana A, "A Thermodynamically Consistent Model for Viscoelastic Polymers Undergoing Microstructural Changes" International J. Engineering Science, 142, pp. 106-124, 2019
- 27. Song R, Berer M, and Muliana A (2022), "Mechanical Responses of Semi-crystalline Thermoplastic Polymers at Various Temperatures" International Journal of Solids and Structures, in press
- 28. Taylor, R.L., Pister, K.S., and Goudreau, G.L. (1970), "Thermomechanical Analysis of Viscoelastic Solids," Int. Journal for Numerical Methods in Engineering, Vol. 2, pp. 45-59
- 29. Tscharnuter, D and Muliana AH (2013), "Nonlinear Response of Viscoelastic Polyoxymethylene (POM) at Elevated Temperatures" Polymer, 54, pp. 1208-1217
- 30. Vannoni M, Sordini A, and Molesini G (2011), "Relaxation Time and Viscosity of Fused Silica Glass at Room Temperature" European Physics Journal E, 34: 92
- 31. Williams, G. & Watts, D. C. (1970). "Non-Symmetrical Dielectric Relaxation Behavior Arising from a Simple Empirical Decay Function". Transactions of the Faraday Society. **66**: 80–85
- 32. Xu Q, Engquist B, Solaimanian M, and Yan K (2020), "A New Nonlinear Viscoelastic and Mathematical Solution of Solids for Improving Prediction Accuracy" Scientific Reports, 10, 2202
- 33. Yao W, Dagang S, Zhanlong L, Yuan Q, Bao S (2021) "A variable-order viscoelastic constitutive model under constant strain rate," J. Transactions Canadian Society for Mechanical Engineering, 45(3): 355-362
- 34. Yuan L and Agrawal OP (2002), "A Numerical Scheme for Dynamic Systems Containing Fractional Derivatives" J. Vibration and Acoustic, 124, pp. 321-
- 35. Zhang W, Capilnasiu A, Sommer G, Holzapfel GA, Nordsletten DA (2020), "An Efficient and Accurate Method for Modeling Nonlinear Fractional Viscoelastic Biomaterials" Computer Methods in Applied Mechanics and Engineering, 362, 112834

Tables

Table 1 Time-dependent parameters from one dimensional fractional viscoelastic model

	<i>N</i> =1	<i>N</i> =2
$D_{\beta_{\mathrm{l}}} (\sec^{-\beta_{\mathrm{l}}})$	0.05	0.0262
$eta_{ m l}$	0.25	0.3
$D_{\beta_2}(\sec^{-\beta_2})$		0.02
β_2		0.08

Table 2 Prony parameters from one dimensional classical viscoelastic model

N_p	$\tau_n(\mathrm{sec})$	D_n
1	10	0.02
2	100	0.1
3	1000	0.13
4	10000	0.31
5	100000	0.66

Table 3 Time-dependent parameters from different trials

	Trial 1	Trial 2	Trial 3
$D_{\beta_1} (\sec^{-\beta_1})$	0.0262	0.0262	0.0325
eta_1	0.3	0.3	0.28
$D_{\beta_2}(\sec^{-\beta_2})$	0.02	0.01	0.01
β_2	0.08	0.15	0.15
RMS	0	0.0047	0.0069

Table 4 Time-dependent parameters from multi-axial fractional viscoelastic model

$B_{\delta_1} (\sec^{-\delta_1})$	0.05	$J_{\lambda_{\rm l}} (\sec^{-\lambda_{\rm l}})$	0.025
δ_1	0.11	λ_1	0.13
$B_{\delta_2}(\sec^{-\delta_2})$	0.033	$J_{\lambda_2}(\sec^{-\lambda_2})$	0.035
δ_2	0.3	λ_2	0.29

Table 5 Computational time (unit is in second)

$\Delta t (\mathrm{sec})$	Fractional Model	Classical Model
0.1	22870.17	0.9826
0.2	5817.83	0.1056
1.0	235.97	0.031
2.0	58.52	0.02
5.0	9.33	0.014
10.0	2.33	0.0139

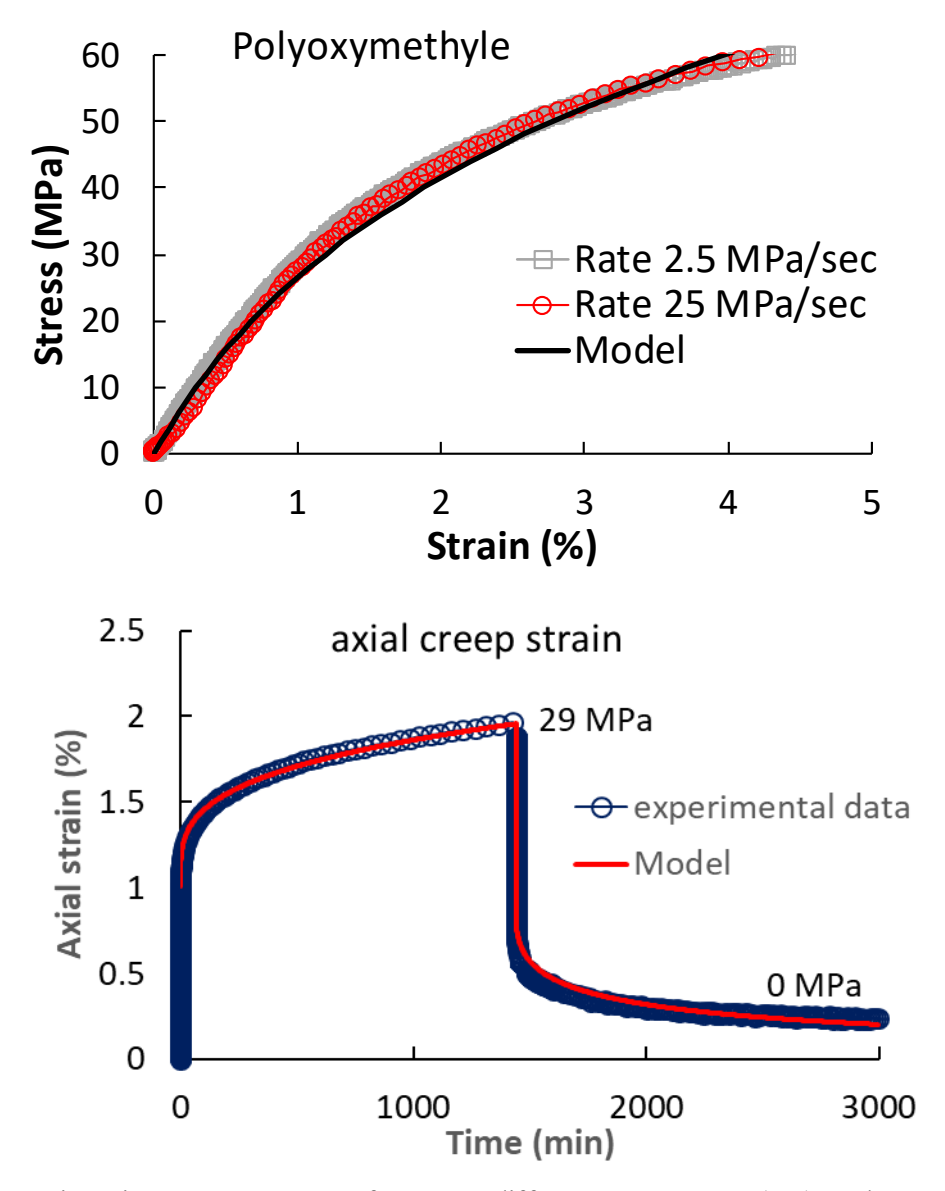


Figure 1 Quasi-static ramp response of POM at different stress rates (top) and Creep-recovery response of POM (bottom)

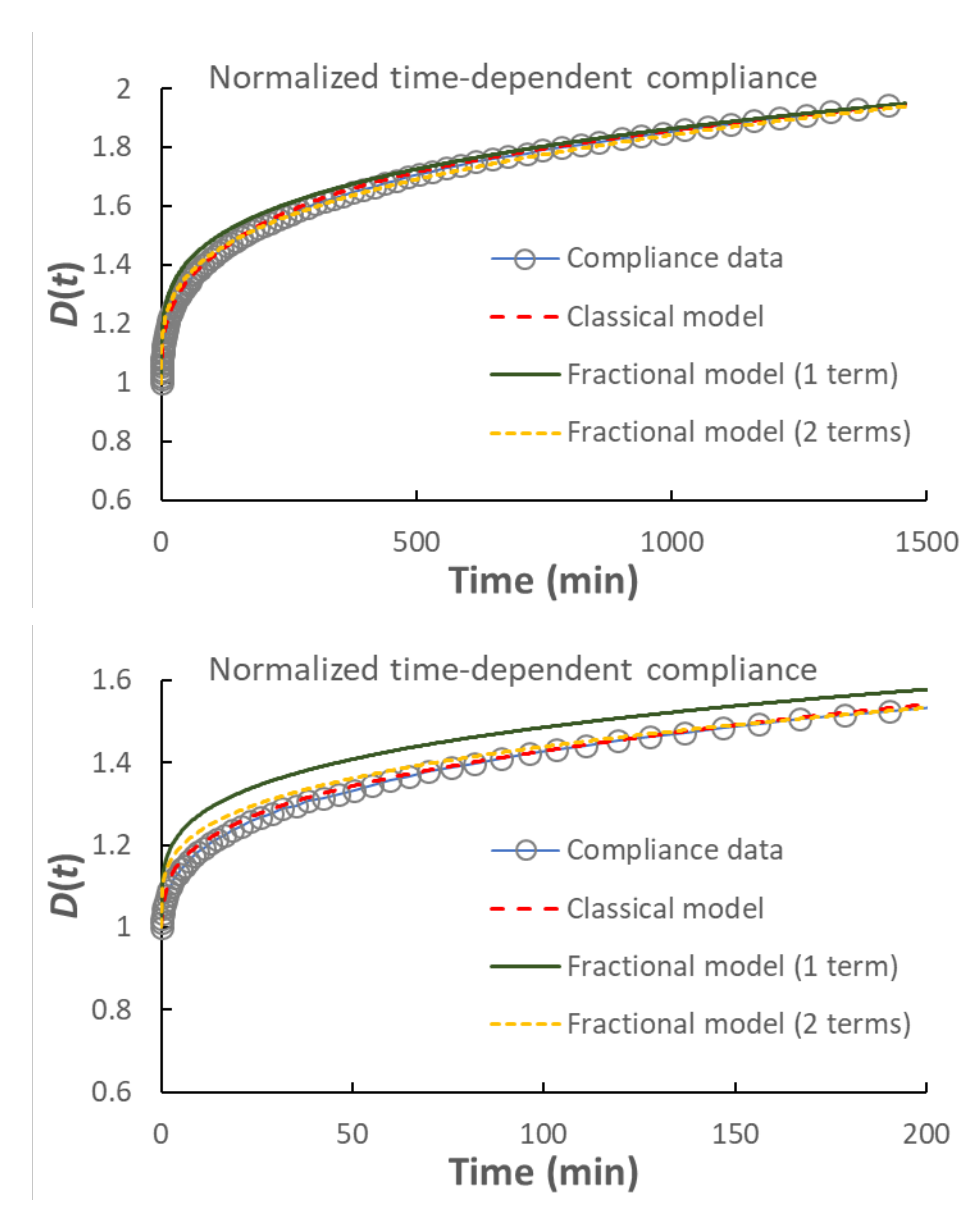


Figure 2 Creep compliance responses for the entire test (top) and at early time (bottom)

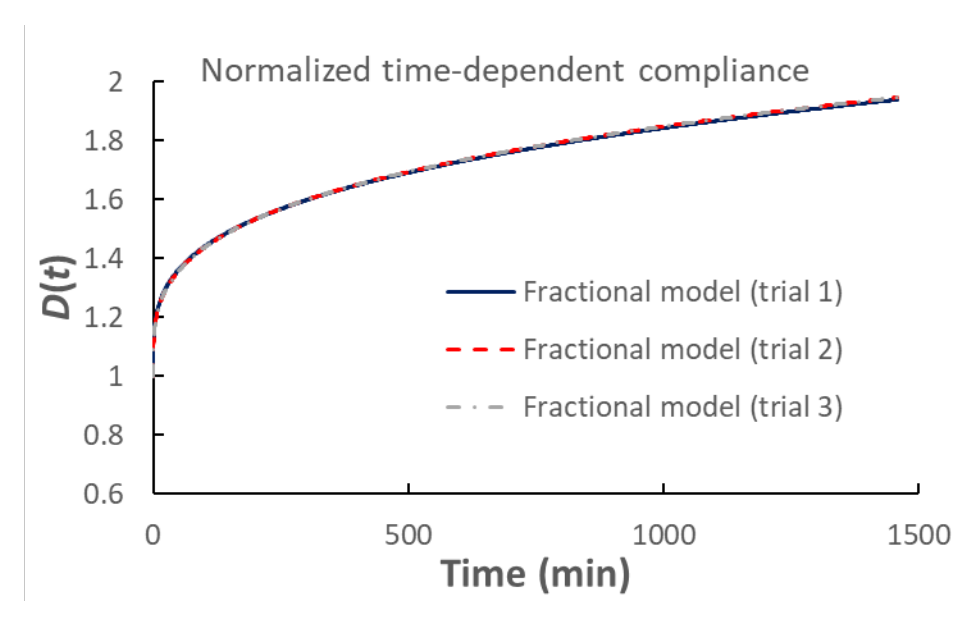


Figure 3 Time-dependent compliances from three sets of material parameters

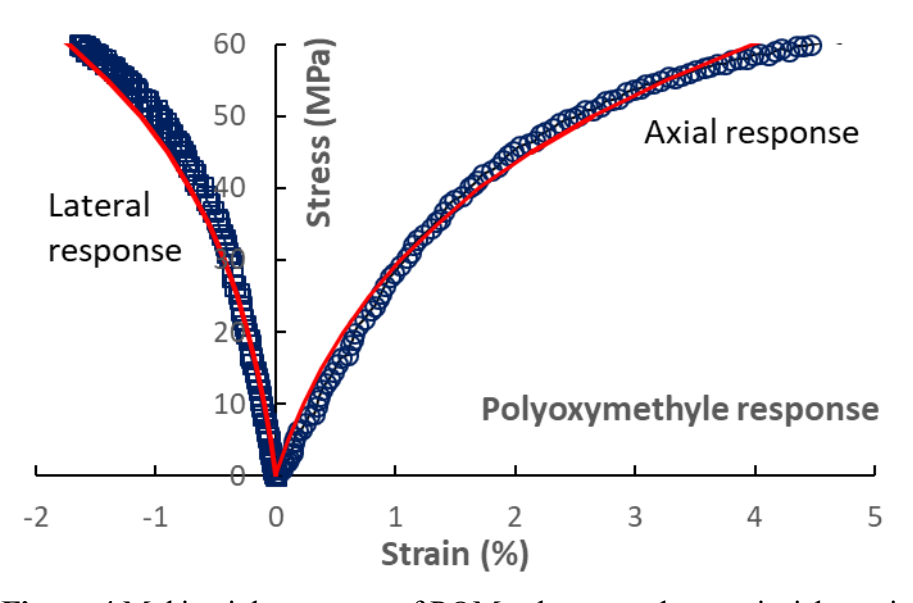


Figure 4 Multi-axial response of POM polymer under a uniaxial tension

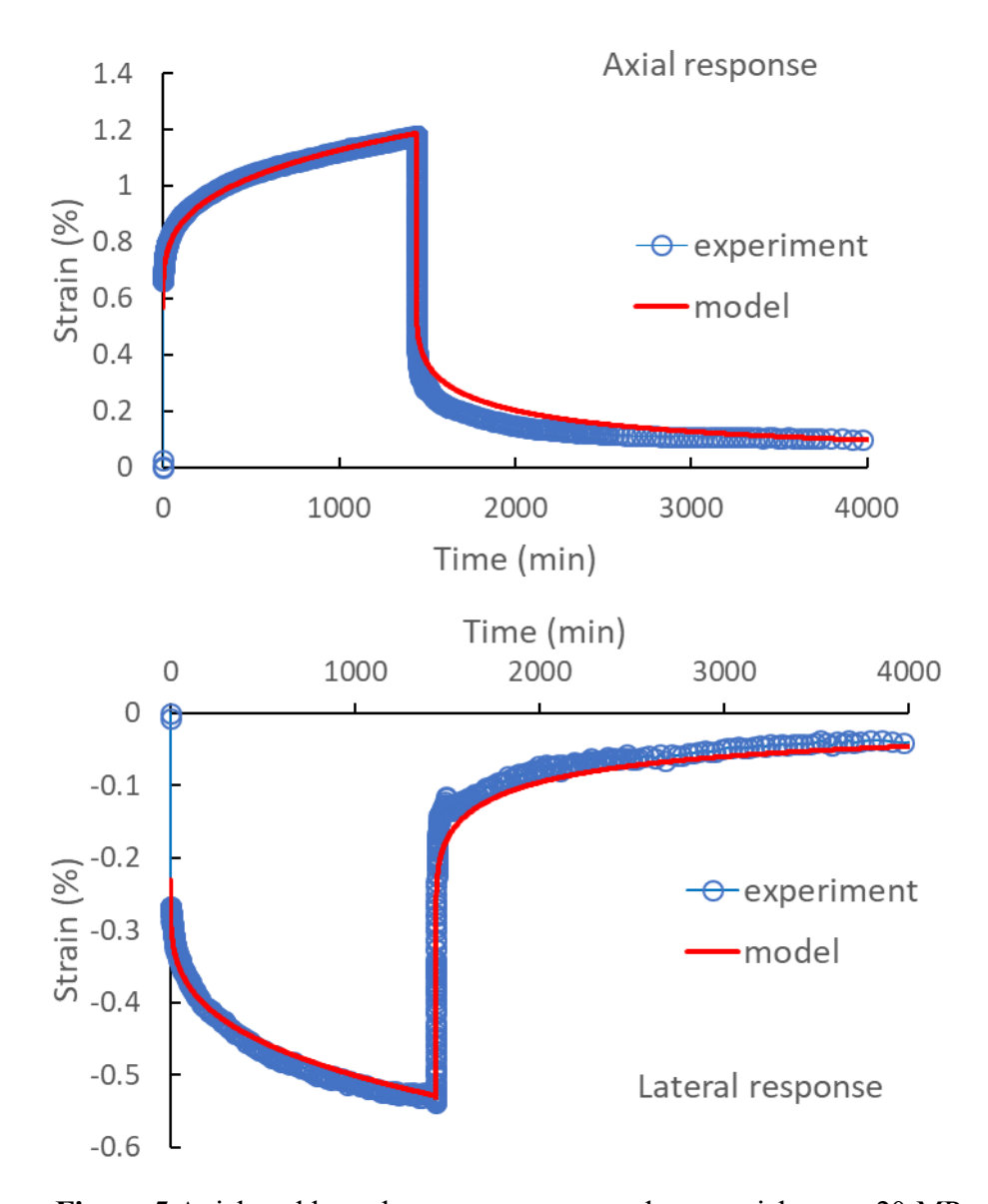


Figure 5 Axial and lateral creep responses under an axial stress 20 MPa

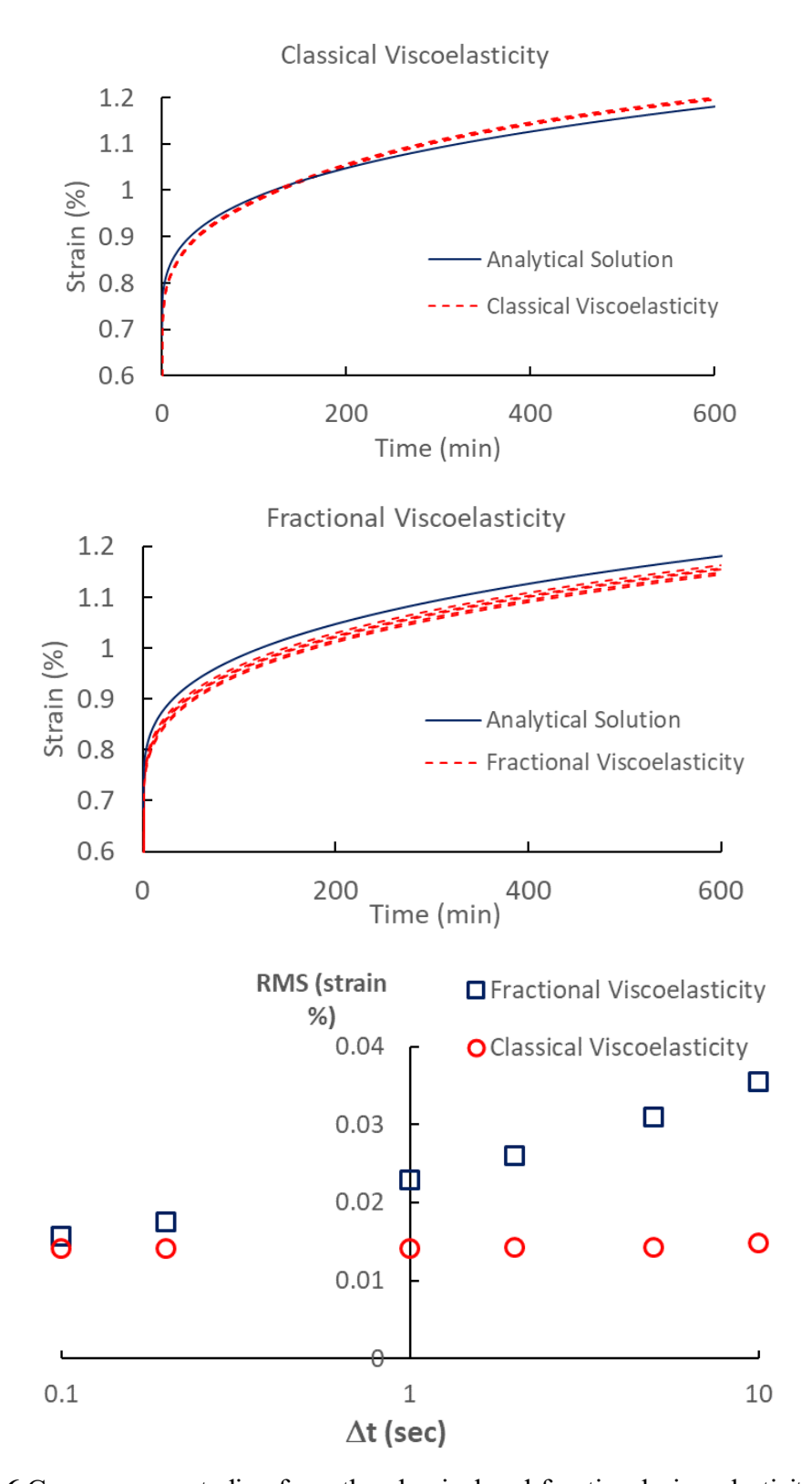


Figure 6 Convergence studies from the classical and fractional viscoelasticity models

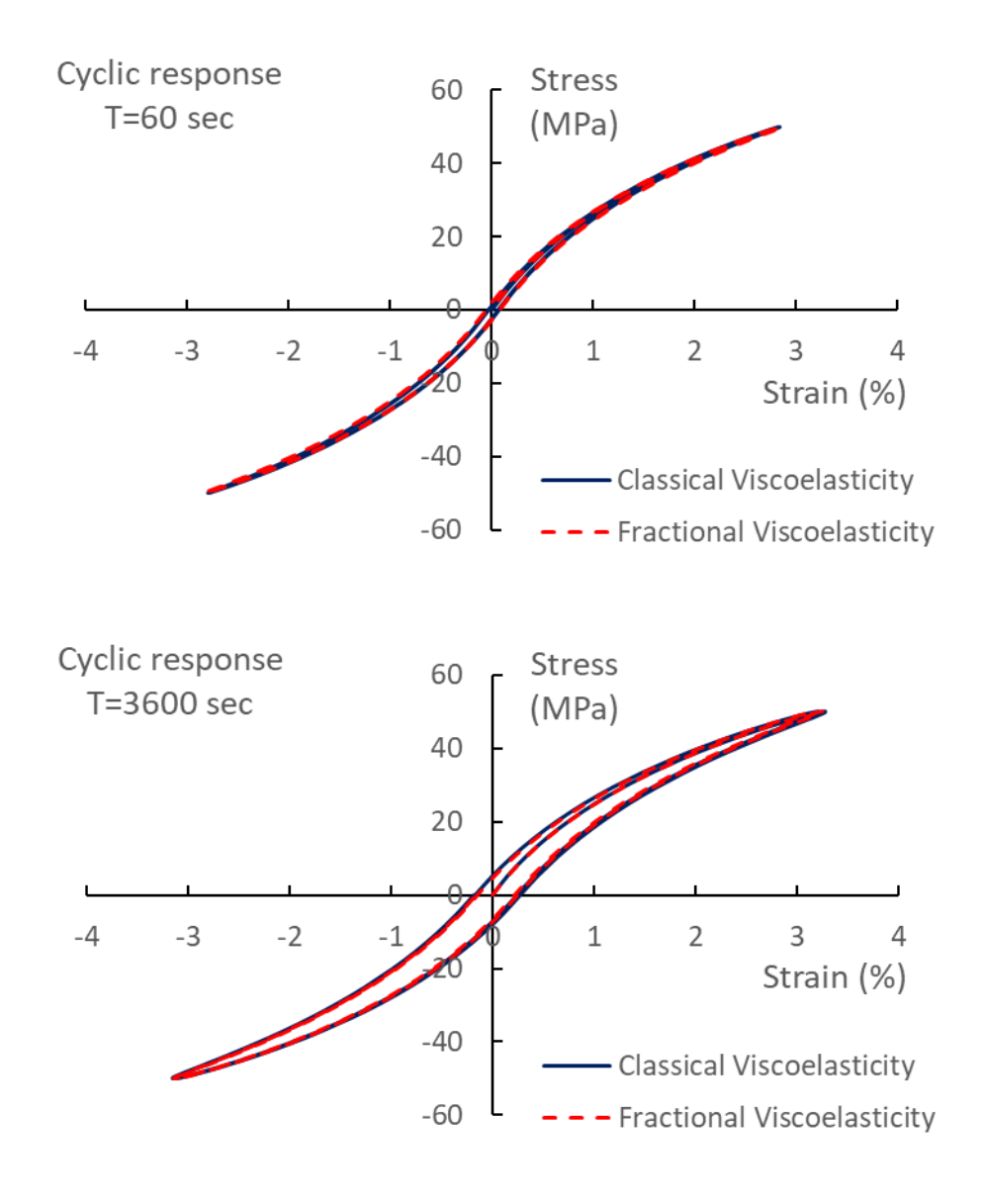


Figure 7 Cyclic responses at two different periods

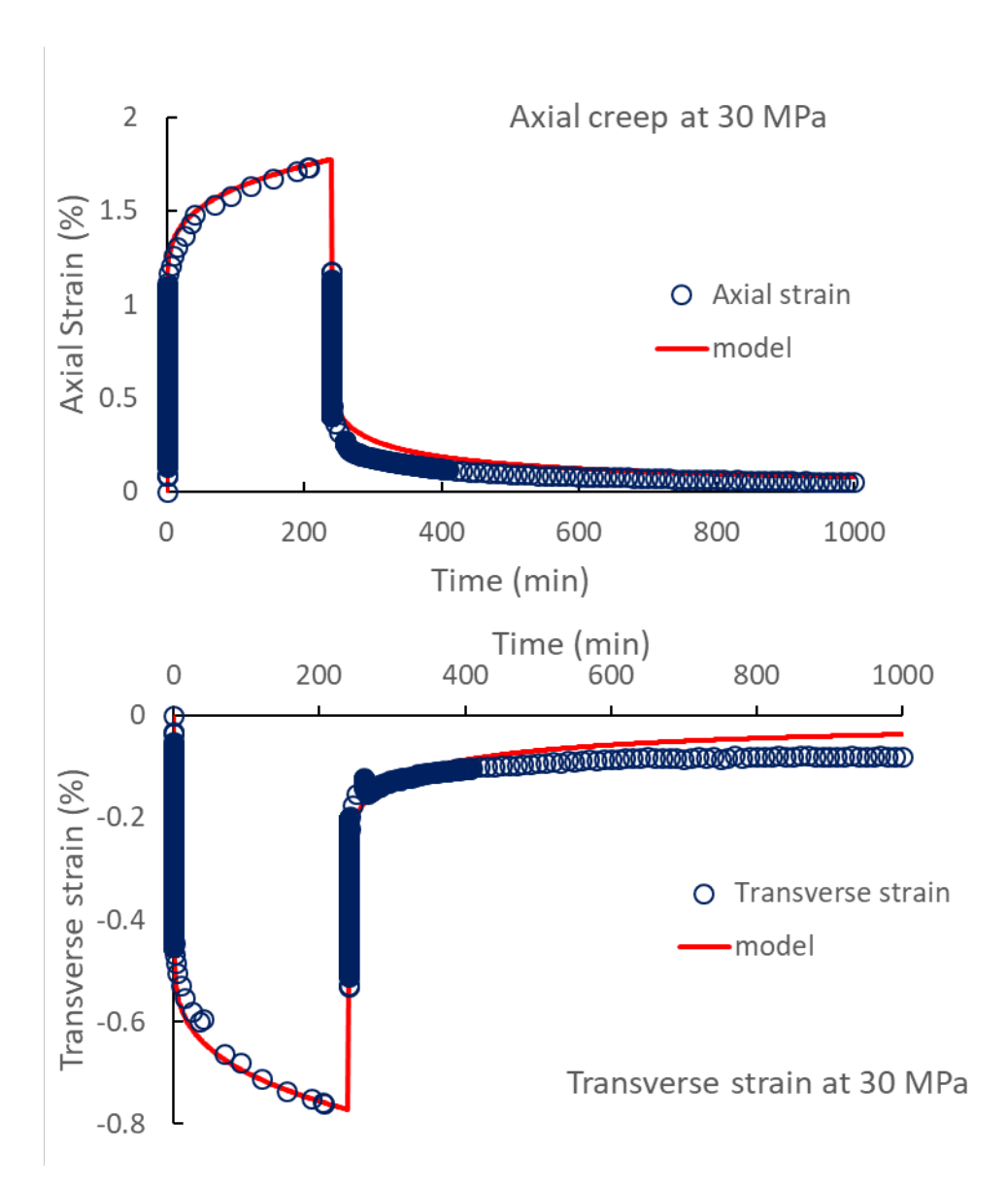
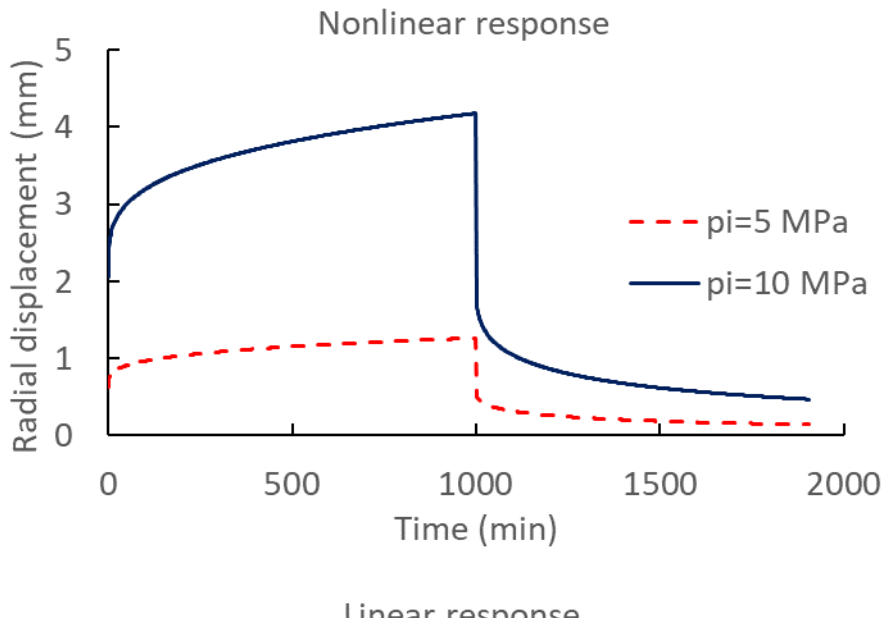


Figure 8 Multi-axial creep recovery predictions of the nonlinear fractional viscoelastic model



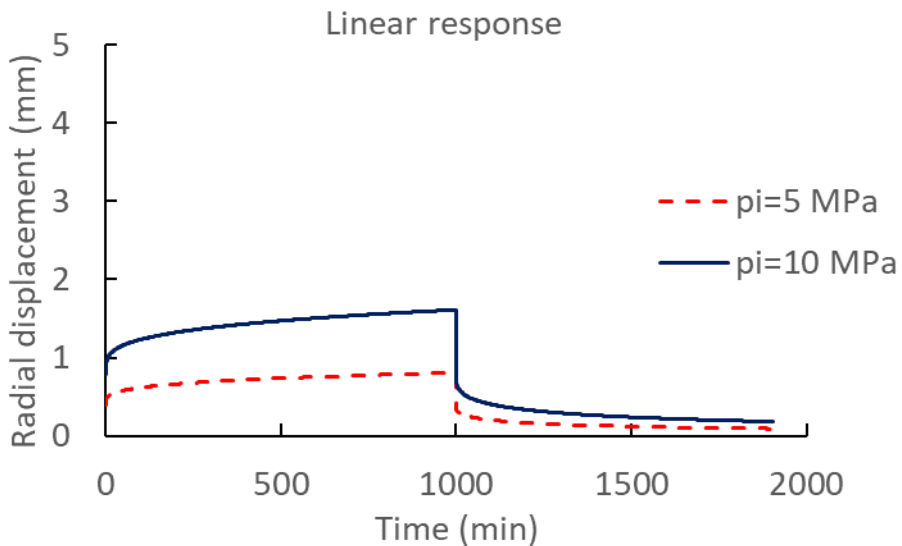


Figure 9 Inner radial displacement responses

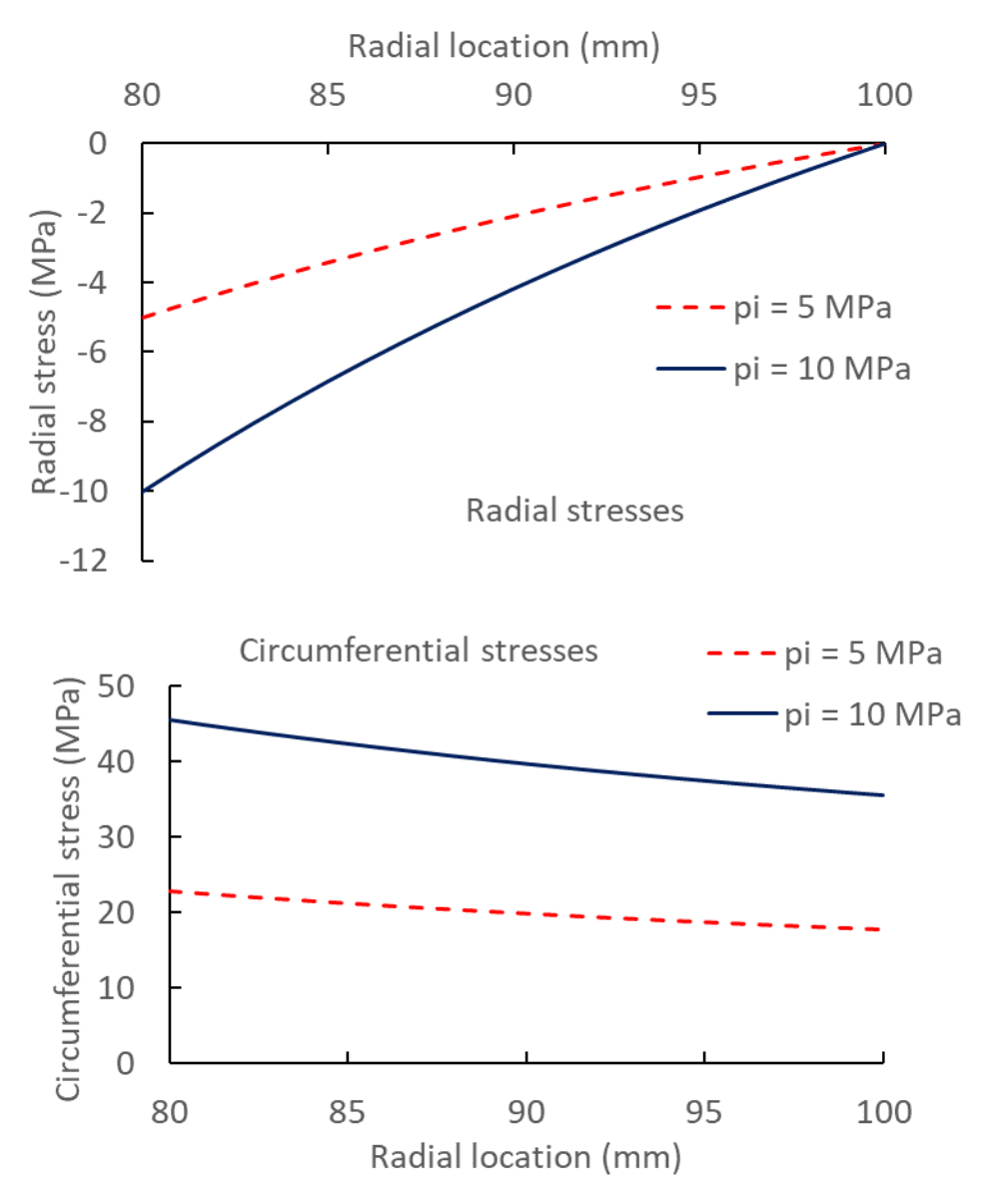


Figure 10 Spatial distributions of radial and circumferential stresses

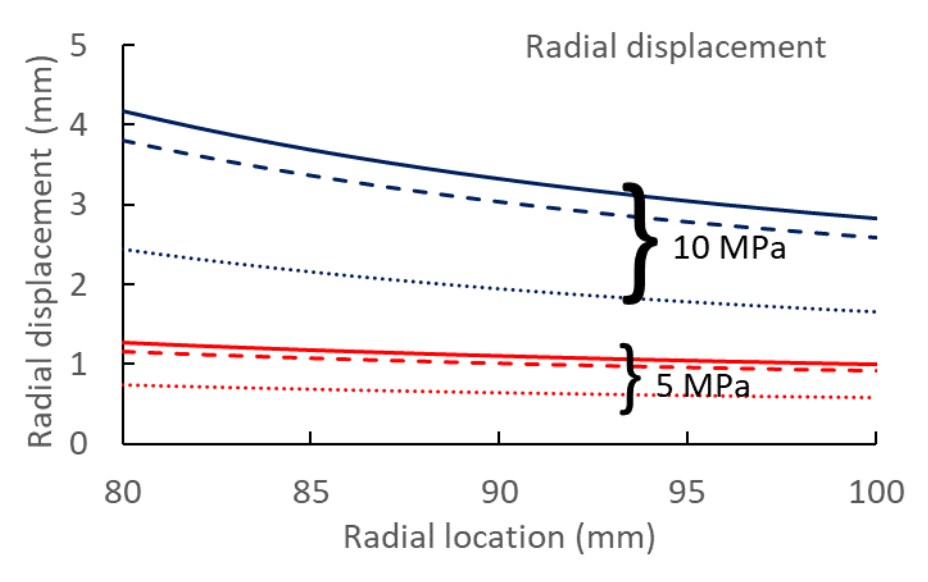


Figure 11 Spatial variation of radial displacements at two inner pressures at times 1 (dotted line), 500 (dashed line), and 1000 (solid line) minutes

Appendix Experimental Study on Polyoxymethylene (POM)

The investigated polyoxymethylene (POM) is Tenac 3010 produced by Asahi Kasei Corporation (Tokyo, Japan). ISO 3176 type B specimens were injection-molded (Tscharnuter and Muliana 2013). The POM specimens were subjected to uniaxial tensile tests under various histories: quasistatic ramp loadings with constant strain rates and creepunder constant stresses as well as recovery tests. Tensile tests at room temperature with constant rates of 2.5 and 25 MPa/sec were performed using an MTS servohydraulic testing machine. The creep tests were performed using force control with initial loading at a prescribed force rate. The recovery from monotonic tension was measured directly on the testing machine. Due to the extensive duration of the recovery, which was monitored for 2.5 months after 24 and 72 hours of creep, the recovery of the strain associated with the viscoelastic response was measured on a separate device. Axial and transverse strains were measured using the digital image correlation system ARAMIS (GOM mbH, Germany. For this study, the measurement was performed in three-dimensional (3D) mode using 105mm lenses. Detailed discussion on the experimental tests can be found in Tscharnuter and Muliana (2013).

Data Availability Statement

Data available on request from the authors.